# Rotational Distributions in Vibrational Transfer†

**Anthony J. McCaffery* and Richard J. Marsh**

*School of Chemistry, Physics and Environmental Science, University of Sussex, Brighton BN19QJ, U.K.*

*Received: April 3, 2000; In Final Form: June 20, 2000*

Rotational distributions vary widely among the different collisional interactions that initiate chemical and physical change, processes that are often regarded as differing in kind. Here the *commonality* of mechanism among a variety of collision-induced processes is emphasized. This mechanism is the conversion of linear-to-angular momentum at the hard wall of the intermolecular potential. Its operation is constrained by (i) the existence of quantized molecular eigenstates and (ii) boundary conditions set by energy conservation. The wide variation of these boundary conditions under differing kinematic circumstances gives rise to the wide variety of rotational distributions that is observed experimentally. Three cases of vibrotation transfer (VRT), namely $Li_2$−Ne, NO−NO, and HF−H are considered in detail. It is shown that the natural distribution in VRT is best described as "frustrated exponential-like", only recognized as such by observing the development of rotational distribution shape as the vibrational momentum "gap" steadily increases, as in the cases considered. The low $\Delta j$ region of the distribution becomes severely truncated as this gap increases, giving distribution shapes which are superficially Boltzmann in appearance. The analysis here indicates that derivation of rotational "temperatures" based on this apparent similarity is likely to give misleading results. Velocity−angular momentum diagrams are used to give physical insight into the operation of the mechanism, the effect of energy boundary conditions and to predict rotational distribution shapes and peak values. The analysis also suggests that in determining vibrational transfer cross section, inaccurate results will generally result unless initial rotational state $j_i \simeq 0$ and the whole manifold of rotational states in $v_f$ is summed.

## 1. Introduction

Theoretical and experimental studies of collision-induced vibrational and of rotational state change have tended to develop along quite separate pathways.[1] Although there are practical reasons why this has occurred, the categorization of different modes of collisional behavior may have inhibited formulation of more general theories embracing *all* forms of collision. Rotational and vibrational transfer (RT and VT) are a case in point. Indeed, it is not uncommon[2] to subdivide VT according to whether the colliding species is monatomic, diatomic, or polyatomic with different models for each. Yet as Murrell and Bosanac[3] state, "rotational and vibrational inelastic processes always go together ...". A corollary is that quantitative measure of the probability of vibrational transfer requires a sum over *all* rotational states populated within a particular vibrational manifold. This appears to be undertaken in experiments only rarely and therefore measurements made without full $j_f$ resolution will generally represent an underestimate of true VT cross sections. Furthermore, as discussed in more detail below, the effect of *initial* rotational state(s) selection cannot be discounted in quantitative determination of vibrational transfer (VT) probabilities.

A striking feature of *vibrotational* transfer (VRT) when rotational states are fully resolved, as they are in some instances, is the marked difference in their distributions among the final $j$ states compared to the case of pure rotational transfer (RT). The characteristic rotational distribution in pure RT is an exponential-like fall of rate constants or cross sections with $\Delta j$. This has been rationalized[5,6] in terms of the shape of the probability density of effective impact parameter (or torque arm) for the conversion of linear-to-angular momentum. The corresponding distributions when VRT occurs will be much influenced by the "momentum gap" that must be overcome to access the vibrational state at the same time as generating torque. An analysis of VRT in the $CO_2$ molecule[7] demonstrates that a shift in the peak of the rotational distribution in VRT will generally take place. This shift may be small when the vibrational "gap" is small but will be quite large when this gap is substantial. Examples exist of both instances and are discussed in more detail below.

The difference in these distributions does not appear to have been previously remarked upon, perhaps a consequence of the separation of the measurement of vibrational transfer (VT) from that of RT as an objective. It should be emphasized that from the point of view of the experimentallist, the determination of full rotational distributions in VT experiments is no trivial matter, particularly for molecules in their ground electronic states. Rotational separations are small and therefore high resolution laser methods are required for this determination, but these devices rarely span the range of wavelengths needed to make a full determination of VRT cross sections. Other factors that inhibit experiment, particularly when based on pulsed lasers, are discussed by Islam and Smith.[8] Nevertheless, the changes that occur in the rotational distributions in differing situations provide key insights into the underlying physics of collisions and measurements of rotationally resolved data are likely to provide a critical test of models.

Here we analyze three sets of data each of which exhibits interesting and unexpected features. The data are first the very detailed and comprehensive sets of VRT rate constants reported by Gao et al.,[9] on $A(^1\Sigma_u^+)Li_2$−Ne collisons involving $v_i = 2-24$, $j_i = 30$. Second are the rate constants reported by Islam

† Part of the special issue "C. Bradley Moore Festschrift".

10.1021/jp001277o CCC: $19.00 
Published on Web 08/19/2000

and Smith for VRT in $X(^2\Pi_{1/2})NO\ (3,j_i)-NO$ collisions. In this work, $j_i = 3, 4, 7, 10, 15$ and $v_f = 2$.[8] The third data set is that reported by Lindner et al.[10] for hot H atom collisions with HF ($v_i = 0$). Models employed by the authors to account for their data vary very widely across the range from impulsive limit using hard ellipsoid shapes to model the repulsive wall in H−HF[10] to full multipolar expansion of the long-range interactions.[8] Gao et al.[9] utilize classical trajectory calculations on an ab initio and on a wholly repulsive surface.

Our approach in analyzing this range of data is to use the model recently introduced[7] in which a common *mechanism* of VRT is momentum transfer which takes place within boundary conditions set by energy conservation. This approach[7] accounts remarkably well for the rotational distributions that accompany vibrational excitation of the asymmetric stretch in $H-CO_2$ collisions.[11] The basis of the method is a modified form of the angular momentum (AM) model of RT introduced by McCaffery et al.[4,5] As in previous papers in this series[7,12−14] we make extensive use of velocity−AM plots, first demonstrated by Besley et al.[15] and used to clarify the underlying physics operating in the case of VRT in $CO_2$[7] in quasiresonant vibration−rotation transfer (QRT) in $Li_2$[7] and in a wide range of other systems.[13]

In doing this, the principal objective is to reveal the mechanism at work and the underlying physical principles. This is much in the spirit of Wodtke and co-workers[16] who assert that "... the most fundamental motivation for studying quantum state resolved energy transfer ... is the prospect of ... obtaining a clear physical picture of the transfer mechanism". The theoretical method we develop here to account for VRT differs only slightly from that used to account quantitatively for the most detailed velocity-, state-, and angle-resolved data in pure RT.[17] A key addition to the basic method that enables VRT to be encompassed is the expression of vibrational motion as (reciprocating) linear momentum.[18] When this is done, the physical basis of VRT[7] and of QRT[12,13] are clearly revealed as are, with only straightforward further modifications, vibrotational distributions in *reactive* collisions.[19]

Here we utilize velocity−AM plots to illustrate the point made in recent analyses of a wide range of collisional processes that the rich diversity of behavior exhibited by the rotational distributions in different forms of collisional transfer arises from the different ways in which the energy conservation relation constrains and moderates the underlying mechanism. This mechanism is *momentum interconversion* (linear to angular and linear to linear *and* angular momentum) at the hard wall of the intermolecular potential. This principle is illustrated in the next section by reference to a number of examples.

## 2. Velocity−Angular Momentum Analysis

Collision-induced RT and VRT are most simply described in terms of a mechanism in which linear momentum is converted to rotational angular momentum (referred to as LM → AM in what follows) on collision through the agency of a torque arm (or effective impact parameter) of molecular dimension. The mechanism operates strictly within *constraints* set by energy conservation and by the quantization of internal states of the molecule involved in the collision.[4,17] LM → AM conversion is very transparently displayed in plots of these two variables, but we have demonstrated in a series of recent publications that considerable insight into factors that constrain the basic LM → AM mechanism is obtained when the energy conservation equation is plotted on the same axes. This is best achieved by choosing velocity and AM as the variables plotted, as shown below. This manner of representation reveals very clearly the circumstances that give rise to deviations from the basic patterns of RT and demonstrates that such deviations invariably stem from the constraints that energy conservation imposes in the fundamental LM → AM mechanism.

As noted in the previous section, the principal objective here is the (qualitative) illustration of the underlying physics of the collisional process in a number of different situations in order that the commonality of mechanism and the variation of the constraint conditions may be highlighted. We have shown in a series of recent papers[7,13,14] that simple hard ellipsoid models for the conversion of LM → AM in conjunction with Monte Carlo simulations of the collision trajectories yield reliable, quantitative values of state-to-state cross sections using only the simplest of calculations. This is found to be the case for pure RT[14] as well as in cases of VRT in linear triatomics[7] and in diatomics.[14] This approach was first introduced by Kreutz and Flynn,[20] though it should be remarked that the multiellipsoid Monte Carlo method of Marks[21] represents a very significant enhancement of that approach. The model is useful in that quantitative predictions are obtained using a representation of the physical dimensions of the molecule in the form of the repulsive wall and its radial and angular variation.

**2.1. Threshold Kinematic Relationships.** The relationships that represent channel opening conditions for the conversion of relative velocity of collision both into rotational (and vibrational) energy and into angular (and linear) momentum are very clearly represented by velocity−AM plots, as first introduced by Besley et al.[15] These plots have been used to illustrate the commonality of mechanism between such diverse phenomena as (i) the rotational distributions following collisional excitation of the (001) mode in $CO_2$,[7] (ii) the reduction of RT rate coefficients with increasing $j_i$ state and with increasing collision-reduced mass in $Na_2$,[14] and (iii) the occurrence of quasi-resonant VRT in a range of light molecules.[12,13] The velocity−AM plots are graphical representations of the following limiting relationships for the conversion of relative velocity of collision ($v_r$) into *change of* rotational AM ($\Delta j$) of the molecule. Note that these equations represent the *threshold* or channel-opening conditions for a particular $\Delta j$ value.

(i) Conversion of relative velocity into change of rotational AM via an effective impact parameter or torque arm ($b_n$)

$$\Delta j = \mu v_r b_n^{\max} \tag{1}$$

Here $\mu$ is collision-reduced mass and $b_n^{\max}$ is the *maximum* value of the torque arm about which LM → AM conversion is effected. Note that we[5] and other authors[22] have found that $b_n^{\max}$ frequently is half the bond length (HBL) of a (homonuclear) diatomic, giving substance to the notion that the physical "shape" of a molecule is of real significance in molecular collision dynamics. Besley et al. have demonstrated that this equation represents the onset of $\Delta j$ channel opening through *forward* scattering via the LM → AM process, and we refer to it as the A equation in what follows.

(ii) Conversion of kinetic energy of relative motion to change of rotational energy

$$\Delta j = -j_i + \frac{\sqrt{(2Bj_i)^2 + 2B\mu(v_r)^2}}{2B} \tag{2}$$

Here $B$ is the rotational constant for the diatomic species. This equation, which is given here for the general case of $j_i \neq 0$, is

referred to in the following as the E equation since it represents the onset of conditions that meet energy conservation.

In other publications[7,14,15] we have also displayed graphical representations of an additional equation representing the channel opening conditions for simultaneous energy and AM conservation, referred to as the (E + A) relation. As described in some detail in those papers, the (E + A) plot represents the onset of channel opening for backward scattering and, for the most part, this process is of inherently low probability except under rather unusual circumstances, which are described in more detail in the references cited. This particular plot in conjunction with the A and the E relationships is useful in predicting angular distributions from scattering experiments, as recently demonstrated.[15]

The primary mechanism by which linear momentum is converted into AM in this model is embodied in the transfer function for RT given by Osborne and McCaffery[5]

$$P(j_f|j_i)\,\mathrm{d}j_f = C\int_0^{b_n^{\max}} P(l|b_n)\,\delta(|E_{\mathrm{tot}} - E'_{\mathrm{tot}}|)\,\delta(|J_i - J_f|)b_n\,\mathrm{d}b_n\,\mathrm{d}j_f \quad (3)$$

The components of this relationship are discussed in detail in ref 5 and are not revisited here except to point out the importance of the quantity $b_n^{\max}$ in determining the overall RT probability. Equation 3 was found to give an excellent fit to all known RT data, and the value $b_n^{\max}$ = HBL is returned again and again from such data.[5] This simple relationship is not invariably maintained and channel-dependent maximum values of $b_n <$ HBL are commonly found, a theme developed more fully in what follows.

In the case of diatomic molecules, eq 3 predicts a probability distribution in $\Delta j$ that is rapidly falling as $\Delta j$ increases, as found experimentally. We refer to this distribution as "exponential-like" in what follows. The experimental dependence on transferred AM was originally suggested to be exponential in form[23] but later shown, after an extensive but entirely empirical examination, to follow more closely an inverse power relation.[24] We have demonstrated[5] that this behavior originates in the functional form of the term $P(b_n)$, which is best represented by $b_n^{-\gamma}$, where $\gamma \simeq 2$. This form was shown[6] to be related to the probability density of repulsive anisotropy, averaging radial and angular contributions. Equation 3 therefore represents the fundamental mechanism of RT. In VRT, a component of initial momentum of relative motion is directed along the diatomic bond and must be sufficient to open the vibrational channel before VRT may occur. In calculations of vibrotational distributions in $CO_2$−H* collisions using a hard ellipsoid model of the intermolecular potential,[7] this vibrational channel-opening velocity is subtracted *vectorially* and the remaining component may be used to open rotational channels. As we have commented in earlier publications,[17] the model is Newtonian in spirit but recognizes constraints imposed by the existence of quantized molecular eigenstates (as well as those enforced by energy conservation). The basic "currency" throughout the collisional "transaction" is *momentum*, therefore, rather than energy.

**2.2. Four Distinct Cases of RT/VRT.** The equations representing the threshold kinematic conditions expressed in the A and E relationships of eqs 1 and 2 are readily displayed in velocity−AM plots, and we have used such plots recently to demonstrate that seemingly very different forms of collisional transfer share a common mechanism. This mechanism comprises momentum conversion within boundary conditions set by energy conservation. The *mechanism* remains unchanged throughout a wide range of collisional processes, but the richness of variety found experimentally and theoretically for different processes arises principally from the different ways in which the mechanism is modified and constrained by energy conservation. In recent work, we have identified four distinct examples of velocity−AM plot that are associated with seemingly very different processes (indeed ones that have been the subject of much speculation concerning the underlying mechanism) but for which the physics is identical with only the energy boundary conditions varying in each case. These four examples are illustrated by velocity−AM plots in Figure 1a−d. Note that except in 1c, only the A and E relationships are plotted for clarity, and in the unmodified A plots shown in this figure, $b_n^{\max}$ is assumed to be the maximum available from the repulsive anisotropy (generally HBL of a homonuclear diatomic).

*Case 1.* The first figure (Figure 1a) is associated with pure RT from $j_i = 0$ (or some low intial rotor state), a process that results in efficient RT with the full torque arm of the diatomic molecule available.[15] Here the LM → AM mechanism is unconstrained by energy conservation for all values of $v_r$ and for all $\Delta j$. RT in these kinematic circumstances is characterized by the exponential-like fall of RT rate constants or cross sections with $\Delta j$. This very characteristic shape has been shown[5,6] to be a consequence of the shape of the probability density function $P(b_n)$, which averages radial and angular distribution of the repulsive anisotropy in a diatomic molecule. This has the form $P(b_n) = b_n^{-\gamma}$ [5] and strongly weights low $\Delta j$ probabilities. This basic form of $\Delta j$ distribution persists through all other examples though is often strongly masked when the energy boundary conditions operate in a manner that restricts the range of values that $b_n$ may take.

*Case 2.* Figure 1b represents pure RT once again, but in this instance the efficiency of the process is impaired by the effects of a dominant energy constraint. This is typical behavior when $j_i \gg 0$ or when the collision partner becomes very heavy, cases discussed in detail in a recent analysis of trends in pure RT in $Na_2$−rare gas collisions.[14] The mechanism of LM → AM may only operate within the bounds of energy conservation, and this is achieved in the kinematic circumstances portrayed in Figure 1b by means of a reduction in the maximum value of $b_n$, in a fashion such that energy and AM conservation requirements are simultaneously met *for each* $\Delta j$ channel.[7,14] The result of this enforced reduction in available values of $b_n$ is a reduction in the efficiency of RT (an outcome well-known experimentally[25]) although the overall exponential-like shape of the $\Delta j$ distribution is preserved. Note that restrictions on acceptable $b_n$ values carry with them the implication of a reduction in possible collision trajectories, a form of stereo*kinematics*.[7]

*Case 3.* The situation for vibration−rotation transfer (VRT) is very different since now there is a momentum "barrier" that must be overcome, to open the vibrational channel, before any AM may be generated *in that vibrational level*. The size of this gap or barrier will be quite variable according to molecule, degree of vibrational excitation, and vibrational mode (in a polyatomic). An illustrative example is shown in Figure 1c, a pattern of kinematic relationships that differs markedly from the pure RT cases in Figure 1a,b. Now $v_r > 0$ for the opening of the $\Delta j = 0$ channel. The unmodified A plot is unphysical for low values of $\Delta j$ and must be modified by reduction in the maximum value of $b_n$. This reduction will be channel-specific, and it is clear that, above a certain $\Delta j$ value, modification in the range of $b_n$ values will be unnecessary and VRT will be unconstrained with $b_n^{\max}$ = HBL. The method of calculating the new reduced maximum $b_n$ values for each channel for the

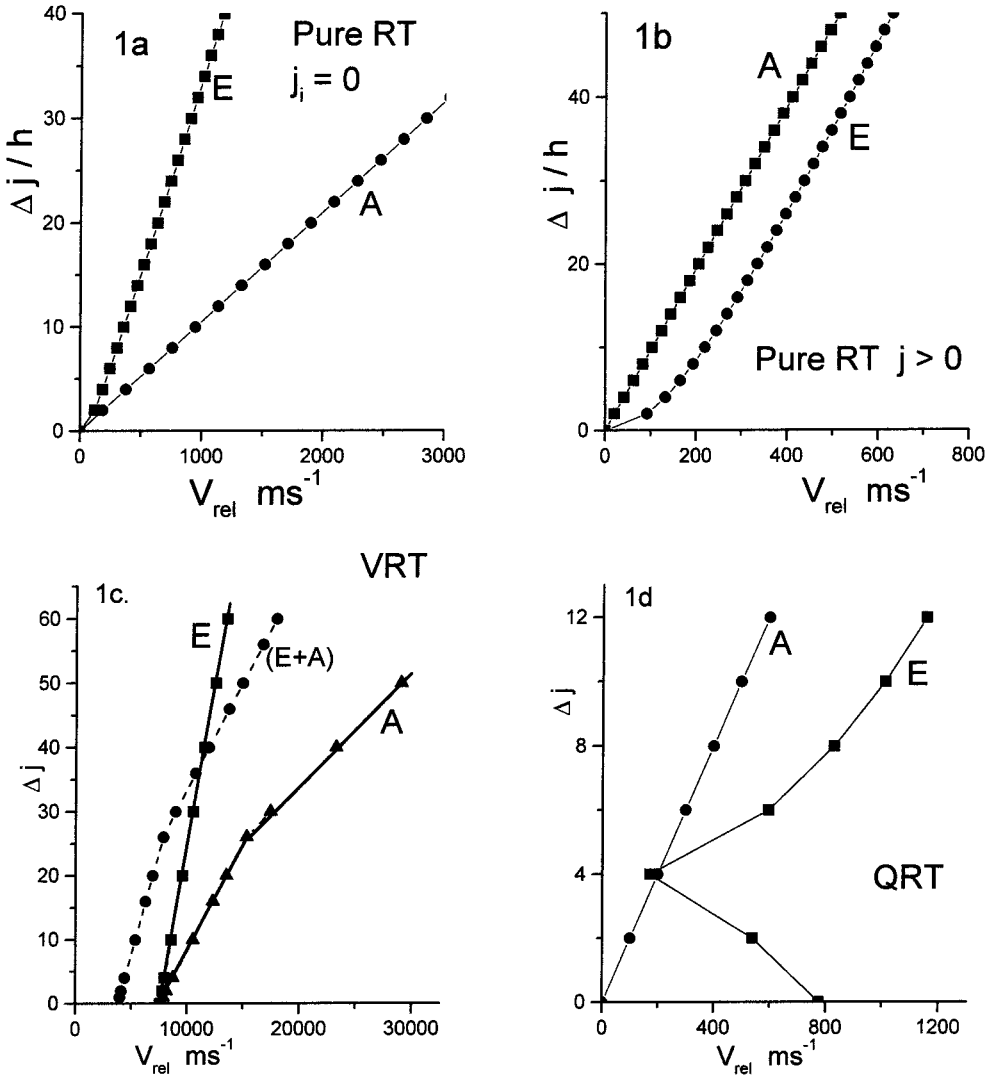


**Figure 1.** Four velocity−AM plots to illustrate the varying E relationship (eq 2) for different collisional processes. As described in the text, this provides boundary conditions within which the mechanism (represented by the A plots) operates and constrains maximum values of $b_n$ for individual channels. Figure 1a shows plots of the E and A equations for pure RT from $j_i \simeq 0$ for low collision-reduced mass. Note that the LM → AM mechanism is unconstrained for all channels in this instance. Figure 1b indicates that the mechanism may be constrained (particularly at low $\Delta j$ when $j_i \gg 0$). This leads to an overall reduction of RT cross sections though the distribution remains exponential-like. Figure 1c shows the (modified) A, E, and (E + A) plots when VRT occurs. There is now a "momentum gap" to be overcome before AM may be generated, and this provides a major constraint on the mechanism for low $\Delta j$ processes. The resultant distribution function of rotational states may be similar to a rotational Boltzmann, but as described in the text, this likeness is superficial. Figure 1d shows the highly characteristic shape of the E plot when quasiresonant transfer (QRT) occurs. The LM → AM mechanism, which is illustrated by the A plot, is constrained at high and at low $\Delta j$ but is unconstrained for a narrow range of $\Delta j$'s, in this instance centered around $\Delta j = 4$. This gives rise to a very sharply peaked distribution of final $j$ states. Further description of each type of kinematic plot is given in the text.

modified A relation (and for the E + A equation) is described in detail in ref 7.

The effect of restricting the $b_n$ values for the low $\Delta j$ channels on the RT rate constants or cross sections depends on the magnitude of the momentum gap. Reference 7 illustrates that for the case of VRT to the (001) level of $CO_2$, there is a dramatic effect. The exponential-like fall of probabilities is totally altered, and the new distribution has a modified Boltzmann-like shape. This comparison is quite misleading since the origin of the VRT distribution is quite unrelated to the physics giving rise to that among thermally populated rotational levels. It is in fact a "frustrated exponential-like" distribution and, as the momentum gap reduces, will revert more and more to the natural form, as we shall demonstrate below. It follows then that the extraction of a rotational temperature via a Boltzmann fit from data of this form will be misleading and temperatures derived from so doing should not be taken literally. Clare et al.[7] show that for VRT to the (001) level of $CO_2$, the peak value of VRT cross-section is shifted from zero (the peak for pure RT) to 16−20. Although the VRT distribution resembles a Boltzmann plot with peak not too far from that appropriate for 300 K, the analysis makes clear that to assign this as a rotational "temperature" would be meaningless since it is a "masked" exponential-like distribution with low values of $\Delta j$ constrained by the energy conservation relation.

*Case 4.* The plot of kinematic relationships shown in Figure 1d is particularly instructive since it is characteristic of an effect that represents a quite spectacular demonstration of the influence of very narrowly defined energy bounds on the LM → AM mechanism. Plots of this form are associated with VRT from high vibration−rotation levels of light species.[12,13] The very narrow region of energy allowedness to the unconstrained LM → AM mechanism arises when energy change and AM change occur in opposite *directions*.[12,13] An essential element is

quasiresonance both in energy *and* in AM, and these are found occurring together only in light diatomics, the hydrides being particular examples. Note that outside the energy-allowed region, the exponential-like decay of $\Delta j$ values is again frustrated or masked as a result of restrictions on $b_n$ values for these channels. Experimental manifestation of these unusual kinematic conditions are the very sharp rotational distributions found in A state $Li_2$-rare gas collisions by Stewart et al. where VRT with $\Delta j = 4$ from, e.g., $j_i = 64$ has a particularly large cross-section.[12] At higher $j_i$ values, $\Delta j = 2$ resonances are predicted[13] with correspondingly larger cross sections.

### 3. Analysis of Rotational Distributions in VRT

The exposition given in the previous section, of four limiting cases of kinematic relationships and the rotational distributions they give rise to, allows us to examine examples of experimental rotational distributions in VRT data and to rationalize these using velocity−AM plots. Note that here we do not attempt to calculate these distributions since the objective here is to display the operation of the constrained LM → AM mechanism in a range of contexts in order to emphasize commonality among collison processes. We have shown that the nested ellipsoid model of Marks,[21] which reproduces RT cross sections quantitatively, also accounts very well for VRT distributions when the physical elements outlined here are incorporated. As these ellipsoids are readily constructed, accurate predictive calculations may be performed very rapidly.

**3.1. VRT in $(A)^1\Sigma_u^+$ $Li_2$−Ne Collisions.** The most complete data sets for atom−diatom rotational distributions in VRT processes are those reported by Stewart and co-workers[9] using high-resolution laser-induced fluorescence. These data are ideal for testing the mechanism proposed since they cover a wide range of $v, j$ states and the experimental uncertainties are small. The work represents one of the few instances in which VT rate coefficients are presented that are sums over entire rotational arrays. The collision energy is fixed for all determinations as is the value of the initial rotor state.

Figure 2a shows a plot of the kinematic equations of this collision pair for the process $v_i, j_i = 12, 30 \rightarrow v_f, j_f = 11, \Delta j$. Comparison with the four separate cases identified in the previous section and illustrated in Figure 1 suggests that there are elements of more than one of the four basic forms contained in the A and E relationships presented here. Thus, in the E plot of Figure 2a, the region below $\Delta j = 8$ is reminiscent of the behavior shown in Figure 1d and characteristic of systems giving rise to QRT. As explained in the previous section, the mechanism of LM → AM, which is forced to operate strictly within the bounds of energy conservation, is restricted in the values of $b_n$ that may be accessed, and thus there is a truncation or masking of low $\Delta j$ values. Figure 2a shows the peak of the velocity distribution in this case, indicating that in this system, for which the momentum gap to open the $\Delta v$ channel is relatively small, there will be a range of velocities that can contribute to low $\Delta j$ channels. The VRT probabilities for low $\Delta j$ will not be negligible; therefore, on the other hand, an exponential-like fall in this region is *not* predicted.

Above $\Delta j = 8$, the E plot in Figure 2a begins to resemble those shown for in Figure 1a,b and characteristic of pure RT. The relative positions of the E and A plots in Figure 2a tell us that the LM → AM mechanism will not be entirely unconstrained above $\Delta j = 10$ but, in analogy to the outcome of kinematic conditions represented in Figure 1a,b, an exponential-like fall of rate constants for values of $\Delta j$ *above* the turn-around region of the E plot in Figure 2a would be anticipated. What

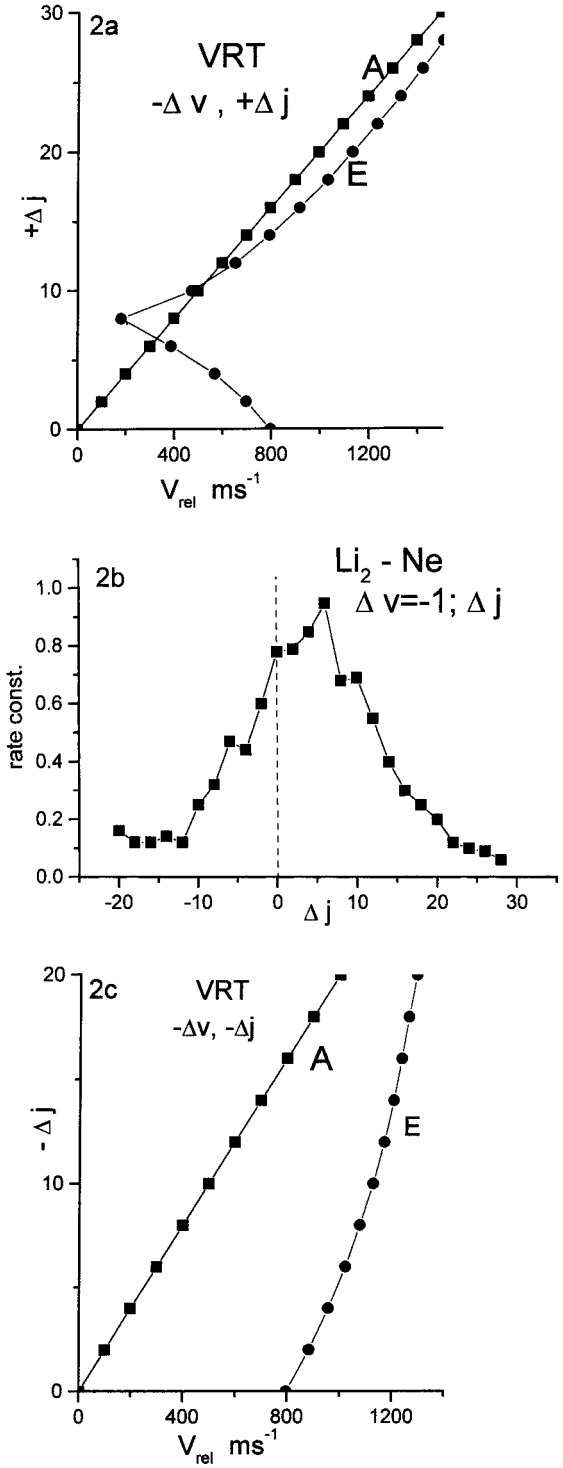


**Figure 2.** (a) (Unmodified) A and E plots for $(-\Delta v, +\Delta j)$ collision-induced transitions in $(A)^1\Sigma Li_2$−Ne. It is evident from this figure that low $\Delta j$ transitions will be suppressed and that the peak of the rotational distribution will be shifted to around 6. (b) Representation of the experimental data, replotted from ref 8, confirming the prediction above. (c) Kinematic equations plotted for $(-\Delta v, -\Delta j)$ transitions and, by analogy to the cases represented in Figure 1, exhibiting a much reduced exponential-like decay.

kind of net pattern of rotational distribution does the velocity−AM plot predict? Bearing in mind the natural exponential-like fall of RT probabilities for the LM → AM mechanism in the unconstrained condition together with channel-dependent restrictions on the maximum value of $b_n$ for $\Delta = 2$, 4 and, to a much lesser degree, 6, the channels $\Delta j = 6$, 8, 10 will be least

affected by energy constraints. Unconstrained RT rate coefficients fall rapidly with magnitude of transferred AM, and with this in mind, together with the kinematic relationships portrayed in Figure 2a, the peak of the rotational distribution for $\Delta v = 1$ is readily predicted to be at $\Delta j = 6$.

Figure 2b is a plot of the rate constants for the process (12, 30) → (11, $\Delta j$) taken from the data of Gao et al.[9] The principal features described in the previous paragraph, deduced from the form of the A and the E plots together with the knowledge of the "natural" or unconstrained rotational state distribution, are seen to give a remarkably accurate picture. This is to be set in the context of equally accurate predictions of VRT distributions in $CO_2$[7] and of QRT in $Li_2$[12,13] using the kinematic approach outlined here. It is straightforward to extend the method to the $\Delta v = -2$ distributions that are also reported by Gao et al.[9] Here the masking effect at low $\Delta j$ is more marked and the peak of the distribution is predicted to shift to around 10, as indeed found experimentally.

Collisional processes that may be represented as being simultaneously ($-\Delta v$, $+\Delta j$) or alternatively ($+\Delta v$, $-\Delta j$), exhibit a pattern of E plot behaviour similar to that in Figure 2a (a $-\Delta v$, $+\Delta j$ process). The distributions here are also readily predicted and indicate that shifts in distribution peak can also be anticipated in this instance. It is worth emphasizing once again that the principal objective in this contribution is to reveal the physical mechanism that is operational in collisional transfer and to have a rule-of-thumb guide to the distributions and the factors governing them. A full picture of the distribution may be obtained from very simple calculations using a hard ellipsoid representation of the repulsive wall. A good example of this is the method described by Kreutz and Flynn,[20] but note that Marks[21] has found that a single ellipsoid representation does not allow a full representation of the small $b_n$ region of the $P(b_n)$ function and hence rarely predicts the exponential-like decay of pure RT rates that is found experimentally.

Gao et al.[9] report VT rate coefficients that sum the rotational distributions, and in light of the foregoing, this can be seen as a welcome development. However, the choice of $j_i = 30$ mitigates against the determination of true RT rates. This is because energy constraints intrude more and more into the region of velocity−AM space that the RT mechanism occupies and rate constants may be much reduced compared to the case when $j_i \simeq 0$. This was emphasized by Parmenter and co-workers recently[25] and was shown[14] to be an instance where the energy boundary conditions in pure RT force a reduction in the maximum value of $b_n$. This reduction is less marked for a light collision partner such as Ne compared with, e.g., Xe, but the increase in energy gap for a given $\Delta j$ change is an inevitable consequence of choosing large $j_i$. The effect of heavy collision partner is to shift the A plot markedly to the left in velocity−AM space and thus hasten the onset of energy constraint.[14]

Finally in this study of the collision dynamics of excited $Li_2$, we turn to the $\pm\Delta v$, $\pm\Delta j$ processes and show kinematic plots for (12, 30) → (11, $-\Delta j$). As is immediately obvious from Figure 2c the E relationship now has a very different form compared to that for the corresponding $+\Delta j$ curve shown in Figure 2a. On referring to the "standard types" discussed above, it is most similar to Figure 1c, which is that characterizing VRT. The rotational distributions in such circumstances have suppressed low $\Delta j$ probabilities,[7] which may be accompanied by a recovery of probability as $\Delta j$ increases if the E plot intersects the A curve at a point on the velocity axis that still leaves a significant amount of the velocity distribution available. This occurs in $CO_2$, leading to a peaked distribution that has disconcertingly Boltzmann-like features, which have been commented on in an earlier section. The E plot of Figure 2c does not give this indication, and a somewhat flattened exponential-like fall of rate constants would be predicted. The plot of (11, $-\Delta j$) rate constants shown in Figure 2b bear out these predictions based on the shapes of the A and E relationships and on the velocity profile.

**3.2. VRT in $NO(X)^2\Pi$, $v = 3$−$NO(X)^2\Pi$, $v = 0$ Collisions.** Islam and Smith[8] have reported rotationally resolved rate coefficients for ($v_i$, $j_i = 3$, $j_i$) → ($v_f$, $j_f = 2$, $j_f$) NO in its electronic ground state ($X^2\Pi_{1/2}$), obtained using the IR−UV double resonance method. The collision partner in this case was NO in its vibrational (and electronic) ground state in a thermal distribution of rotational states. Note that rotational states here are denoted by the symbol $j$ to maintain consistency of nomenclature, recognizing that in spectroscopic notation, the symbol $N$ is widely used for this species. Islam and Smith emphasize the difficulties inherent in the simultaneous determination of vibrational and rotational transfer rate coefficients and comment on the paucity of available data[8] that is a consequence of this difficulty. Nevertheless, there are important issues connected with vibrotational transfer in small molecules, particularly those of atmospheric significance, and it is essential to have a basis of experimental data in order to develop understanding of the underlying physics. These points have been made strongly by Klatt et al.[2] and by Wodtke and co-workers.[16]

Rate coefficients for vibrational transfer in atom−diatom collisions are often very small, particularly for high frequency molecular vibrations. However, when other diatomics are used as the collision partner, the process often becomes much more efficient, enabling rotationally resolved data to be obtained. The contrast to the case of an atomic collision partner suggests that vibrational motion in the collider plays a key role, leading to the categorization of this as vibration-to-vibration (V−V) transfer, and a mechanism involving the long-range attractive intermolecular forces has been proposed[8] on the basis of the Sharma−Brau[27] theory. Here we emphasize the universality of the mechanism described in the foregoing sections in rationalizing collisional processes that are often portrayed as differing in kind. We therefore first investigate the effectiveness of the LM → AM mechanism in revealing the underlying physical processes in collision-induced transfer between two NO molecules.[8]

As before, the appropriate velocity−AM diagram provides a basis for understanding the experimental observations and is shown in Figure 3a. Before drawing conclusions regarding the experimental data (Figure 3b), the manner in which velocity distributions are represented in molecule−molecule collisions requires closer analysis. To emphasize the new elements introduced by a *molecular* collision partner, Figure 3a displays an arrow representing the Maxwell−Boltzmann *relative* velocity peak for collisions between NO and an atomic partner having the same mass as an NO molecule at 300 K.

The channel opening condition for (3, $j_i$) → (2, $j_f$) may readily be represented as velocity. In this encounter between two NO atoms, the *partner* NO molecule possesses a characteristic momentum of vibrational motion, as does the target NO species undergoing deactivation. The collision partner in this instance undergoes vibrational excitation $v = 0 \rightarrow v = 1$ at the same moment the target molecule is deactivated. Upon collision, this vibrational excitation provides a very sharply defined impulse that can contribute to de-excitation of the target NO species. This is displayed on the velocity axis together with the distribution due to translational motion.

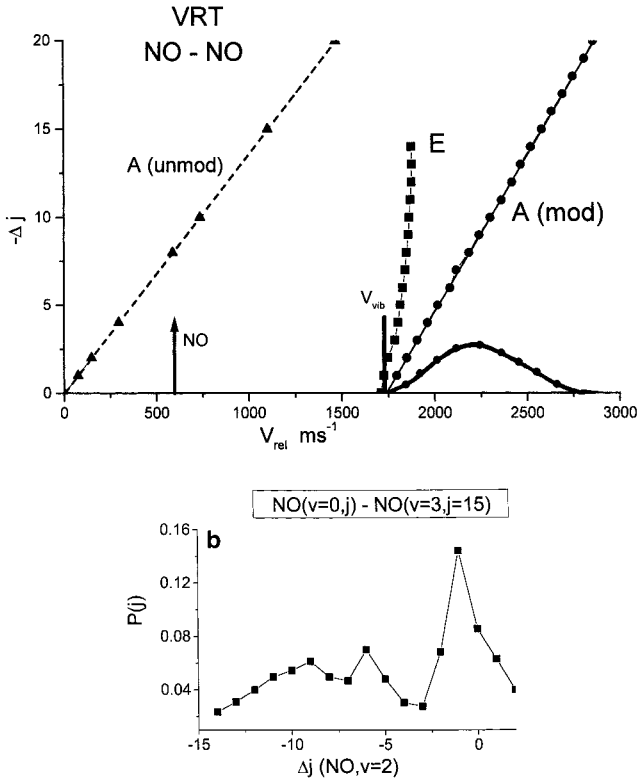


**Figure 3.** (a) Kinematic equations plotted for VRT (3, 15) → (2, Δ*j*) in NO in collision with NO ($v = 0$). Modified and unmodified A relations are plotted to show how the mechanism is changed by the requirements of energy conservation. The E relation is plotted for *negative* Δ*j* only. The figure shows a Maxwell−Boltzmann (MB) distribution of relative velocities for the experimental conditions. This distribution is projected to higher velocities when associated with the velocity of vibrational motion that excitation of NO $v = 0 \rightarrow v = 1$ brings on collision. The latter contribution is represented by a $\delta$ function at 1730 ms$^{-1}$. As seen in the figure, this is coincident with the $\Delta j = -1$ transition and explains the dramatic enhancement of rate constants for this channel. In addition to the enhancement around low Δ*j* values, the modified A plot in conjunction with the MB distribution predicts a broad maximum around 6−10, which is also in line with experimental observations. The arrow shows the MB peak velocity for a reduced mass equivalent to NO−NO collisions. (b) Experimental VRT rate constants (redrawn from ref 2) for the process (3, 15) → (2, Δ*j*) in NO−NO collisions.

In more visual terms, the NO partner molecule's vibrational excitation, when expressed in the common velocity currency employed in the plots, projects the Boltzmann distribution of relative velocity along the velocity axis to a point just *above* (as a result of vibrational anharmonicity) the channel-opening velocity for the NO molecule undergoing deactivation. Note that this takes the *whole distribution* above channel opening since the vibrational momentum may be added to that of relative motion at the moment of impact. In this light, the much enhanced efficiency of diatomic collision partners in vibrational deactivation or activation process is readily understood and predicted. Several authors have stressed the importance of near degeneracy in energy as one of the conditions for efficient V−V transfer.[2,8,16] The analysis presented here supports this as a basic requirement, though only in the sense that energy provides a rough measure of momentum equivalence *in species of similar mass*. For maximum effect, the momentum available from the partner molecule must exceed (by not too large an amount) that required to open the vibrational channel in the target species. Failure to meet this latter criterion may underly the *in*efficiency of $N_2$ in the deactivation of highly vibrationally excited $O_2$ molecules in the experiments of Mack et al.[16] despite achieving the near *energy* degeneracy condition.

**TABLE 1: Upper Limit of $b_n$ for Specified Δ*j* Channels for VRT from $v = 3 \rightarrow v = 2$ of NO in Collision with Ground State NO**

| Δ*j* | $b_n^{max}$/Å | Δ*j* | $b_n^{max}$/Å |
|---|---|---|---|
| 0 | 0 | 16 | 0.257 |
| 1 | 0.0236 | 17 | 0.267 |
| 2 | 0.0458 | 18 | 0.277 |
| 3 | 0.0667 | 19 | 0.286 |
| 4 | 0.0863 | 20 | 0.296 |
| 5 | 0.105 | 21 | 0.305 |
| 6 | 0.122 | 22 | 0.313 |
| 7 | 0.140 | 23 | 0.321 |
| 8 | 0.155 | 24 | 0.33 |
| 9 | 0.17 | 25 | 0.336 |
| 10 | 0.184 | 26 | 0.344 |
| 11 | 0.197 | 27 | 0.351 |
| 12 | 0.210 | 28 | 0.358 |
| 13 | 0.223 | 29 | 0.364 |
| 14 | 0.235 | 30 | 0.371 |
| 15 | 0.246 | 31 | 0.377 |
| | | 32 | 0.39 |

Figure 3a displays plots of the E relation and the A equation, the latter in two forms, the first being the unmodified A equation with $b_n^{max}$ = HBL for all channels (broken line). Quite evidently this unmodified expression does not meet requirements of energy conservation in the region of velocity−AM space portrayed in Figure 3a. The (channel-dependent) revised maximum values for $b_n$ are readily calculated (Table 1) in the manner described in ref 7, leading to the modified A plot shown as a full line in Figure 3a. This now corresponds to the more physically acceptable notion that AM may not be generated in the vibrationally transferred state until the vibrational channel has been opened. The modified A plot now delineates the region within which the LM → AM mechanism may operate (for forward scattering). Thus, if the velocity distribution were no more than the displaced Maxwell−Boltzmann form, then by analogy to the case of $Li_2$−Ne, a "frustrated exponential-like" distribution of rotational levels would be anticipated. As discussed above, this primarily results from the channel dependent restrictions that energy conservation imposes on the maximum values of the torque arm $b_n$. These are particularly severe for the low Δ*j* channels. These restrictions have the effect of reducing the number of allowed trajectories, a process we have referred to as stereokinematics.[7] A shift in the rotational distribution peak away from $\Delta j = 0$ is predicted, and in view of the magnitude of the momentum barrier to be overcome, this is expected to be quite marked.

A new feature is introduced here and is represented as a spike of velocity at 1730 ms$^{-1}$ arising from the NO partner molecule's vibrational motion. This is the principal agent for vibrational channel-opening in NO−NO collisions and has a distorting effect on the region around $\Delta j = 0$. Islam and Smith[8] report that a striking feature of the experimental data is a strong $\Delta j = -1$ propensity that accompanies the $\Delta v = -1$ process for several values of $j_i$, and in all data sets the rate constant for this channel tends to dominate. Figure 3b depicts rate constants for the case $j_i = 15$ ($N_i = 15$ in spectroscopic notation).

Islam and Smith[8] attribute this $\Delta j = -1$ propensity to long-range multipolar interactions with the dipole−dipole term playing a dominant role. This mechanism is also favored by other authors who have reported molecule−molecule VRT.[16] The dipole−dipole interaction would be expected to favor transitions $\Delta j = \pm 1$ equally, and Islam and Smith present arguments to suggest why this is not in accord with experiment.

The Sharma−Brau model has difficulty with high $\Delta j$ transitions, and in NO−NO collisions VRT is detected well beyond $\Delta j = 10$ (Figure 3b). Thus a full description of the experimental observations would require a hybrid mechanism involving long range and short range interactions. Here our objective is the search for *commonality* in mechanism. Introduction of the Sharma−Brau model in V−V transfer invokes a wholly different process, one which differs from that operational in the case of, e.g., NO−He or NO−Ar collisions.

In our kinematic model, the origin of the $\Delta j = -1$ propensity becomes immediately clear from the velocity−AM diagram when the velocity equivalent of the vibrational motion is displayed. The collision partner NO molecule undergoes vibrational excitation from $v = 0 \rightarrow v = 1$ as the target molecule is de-excited from $v = 3 \rightarrow v = 2$. The vibrational excitation is that of the $v = 0 \rightarrow v = 1$ process, which in velocity terms is 1730 $ms^{-1}$, almost identical with that required to open the $\Delta j = -1$ channel in the target molecule. Together with a small amount of the velocity of relative motion, this is able to meet the combined steric and momentum requirements to open simultaneously the vibrational and rotational channels. This latter aspect is discussed in more detail in ref 7 since it is the component of incident velocity along the NO bond that must satisfy vibrational channel opening conditions, the steric requirements for rotational state change being quite different.

The known distribution function of relative velocities and knowledge of the restrictions on $b_n$ values for individual channels (listed in Table 1, and embodied in the modified A plot) make it straightforward to predict the peak of the rotational state distribution for the process (3, 15) → (2, $\Delta j$). As before, the basic exponential-like decay is truncated for low $\Delta j$ as a result of reductions in $b_n$ range that are demanded by energy conservation. The low $\Delta j$ region is expected to be suppressed therefore, though this is to be seen in the context of the impact of the vibrational momentum. A broad maximum in the region of $\Delta j = 6-10$ would be anticipated, in reasonable agreement with observations. The $\Delta j = +$ve rates would, in analogy to the case of $Li_2$ discussed earlier, be expected to slowly decrease in a less severely truncated exponential fashion. The key features of experiment are readily accounted for while retaining the basic mechanism, namely momentum conversion at the repulsive wall within constraints set by energy conservation and found to work well for other collisional processes. The operation of a mechanism involving the long range forces cannot be ruled out. However, it is clear that it is not necessary to invoke a fundamentally different mechanism when vibrotation transfer is induced by a molecule and that the unified picture of collisions may be sustained.

### 4. Vibrotational Distributions in H*−HF Collisions

Lindner et al.[10] have reported rotational distributions in the $v = 1$, 2 levels of the HF molecule as a result of collisions with "hot" H atoms generated by the photodissociation of $H_2S$. FTIR was used to determine the rotational populations, which are reported as relative probabilities. The authors note that, due to a large excess of Ar atoms present in the experiment, successive collisions occur between Ar and H* atoms, and consequently, the velocity distribution of the latter species is ill defined. This leads to imprecision in predicting the peak of the VRT distributions in HF−H* collisions. Despite this it is an instructive case to consider because of the extremely large momentum gap that must be overcome in order to open the vibrational channels.

Experimental data obtained by Lindner et al.[10] are shown in Figure 4a, and the effect of the large channel-opening momentum gap in suppressing low $\Delta j$ values in $v = 1$ is very apparent. The shape of the rotational distribution is reminiscent of that found in $CO_2$−H* VRT collisions.[7] It is by no means obvious that this shape might be derived from one that is fundamentally exponential-like, and the likeness to a rotational Boltzmann is all too evident. Nevertheless, the evidence of the gradual development of this distribution of $\Delta j$ states as the momentum gap increases, demonstrated in the foregoing examples, argues strongly for the interpretation given here that the similarity to a Boltzmann distribution is deceptive. Lindner et al. find evidence for "at least two different mechanisms" and obtain two different rotational temperatures (1200 and 4800 K) from fitting different regions of the VRT distribution. No comment is given on the magnitude of these values or on the remarkable discrepancy between rotational and vibrational "temperatures" in the HF species after collision.

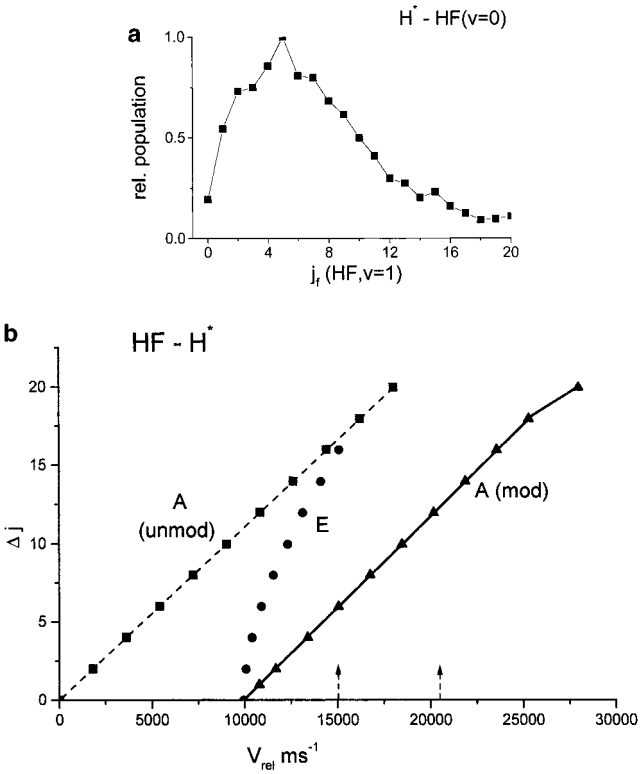


**Figure 4.** (a) Experimental data (replotted from ref 10) showing the distribution of final $j$ states in HF($v = 1$) following collisions between HF($v = 0$) and hot H atoms. (b) Plot of the kinematic relations for VRT in the collision pair HF−H*. Modified and unmodified A plots are shown and the dramatic change brought about by energetic constraints is apparent. In this experiment the velocity distribution is unknown and the arrows mark the extent of this uncertainty. The lower velocity arrow is thought to represent the velocity peak when the first interferograms are recorded, and this predicts peak distribution in good agreement with experiment.

As previously discussed, the momentum analysis presented above indicates that there is no physical basis to the commonly adopted process of extracting a quantity, the "rotational temperature" from fitting a Boltzmann distribution to the rotational populations in VRT unless there is independent evidence of complete thermalization, from examination of the pure RT distributions for example. Energy constraints force suppression of low $\Delta j$ probabilities in VRT, and the result of this is particularly dramatic when the momentum gap is large, as found in HF. The unsuppressed functional dependence on $\Delta j$ is seen in pure RT and is exponential-like.

This becomes apparent when plots of the A and E equations are shown, as in Figure 4b. The figure shows the unmodified

**TABLE 2: Upper Limit of $b_n$ for Specified $\Delta j$ Channels for VRT from $v = 0 \rightarrow v = 1$ of HF in Collision with Hot H Atoms**

| $\Delta j$ | $b_n^{max}$/Å | $\Delta j$ | $b_n^{max}$/Å |
|---|---|---|---|
| 0 | 0 | 10 | 0.357 |
| 1 | 0.061 | 12 | 0.392 |
| 2 | 0.113 | 14 | 0.422 |
| 4 | 0.197 | 16 | 0.447 |
| 6 | 0.263 | 18 | 0.469 |
| 8 | 0.315 | 20 | 0.481 |

A plot that would apply in the case of pure RT and modified A plots that have been made compatible with the energy conservation shown in the E plots using the methods described above and in ref 7. This results in very strong constraints on the maximum values that $b_n$ may take for individual channels listed in Table 2. The result of this is a strong suppression of the low $\Delta j$ probabilities. New threshold relative velocities for rotational channel opening are shown as modified A plots into which the new $b_n$ maxima have been incorporated. These are plotted for VRT to $v = 1$ in HF. In addition, the E equation threshold relative velocity values are plotted for VRT into this vibrational level.

The final piece of data needed to obtain a good rule-of-thumb estimate of the peak of the VRT $\Delta j$ distributions is the distribution function of relative velocity. For experimental reasons alluded to above, this is not readily obtained since the H* atoms from photolysis undergo numerous collisions with Ar prior to meeting an HF molecule. Lindner et al. suggest 1.2 eV as an average collision energy at the time of recording the first interferogram, and this equates to a collision velocity just above 15 000 $ms^{-1}$. Bearing in mind the twin influences of reduced $b_n$ range for low $\Delta j$ due to energy constraints but set against the $b_n^{-\gamma}$ functional form of the $P(b_n)$ density, a peak value of around $\Delta j = 6$ may be read off directly from the modified A plot for $v = 1$. In view of the uncertainties associated with the velocity−AM plots other than to comment that equally accurate estimates of the peak $\Delta j$ values for VRT in DF may also be obtained from the appropriate kinematic plots.

## 5. Conclusions

The analysis of rotational distributions in vibrotational transfer presented here develops further the AM model of collisional phenomena which emphasizes the commonality of mechanism among processes often regarded as wholly different in type. The mechanism, conversion of linear momentum of relative momentum into rotational angular and vibrational linear momentum is moderated by the need (i) to preserve the quantized nature of molecular eigenstates and (ii) to operate within boundary conditions set by energy conservation. The variation of these energy conservation conditions determines the wide variety that is observed in the distributions among rotational states. It is not necessary to invoke differing mechanisms for different collisional processes.

In certain kinematically determined circumstances, the energy boundary conditions impose particular constraints on the LM → AM mechanism such that the range of $b_n$ values is restricted to lie below a maximum value. This upper value of the effective impact parameter may be readily determined from the equations that simultaneously solve for energy and AM conservation. This, in effect, leads to a restriction of trajectories that may lead to successful VRT, a form of stereokinematics to which we have previously drawn attention.[7,14] In this, the *product* eigenstate determines the direction of successful trajectories once velocity is specified. Constraint-induced restrictions on the maximum value of $b_n$ will in general be a particular characteristic of VRT as a result of the momentum gap that must be overcome to open the vibrational channel. The effect is shown to be a truncatation of the low $\Delta j$ probabilities in the rotational distribution to a degree that depends on kinematic factors and the magnitude of the momentum gap needed to open the vibrational channel. This effect has been seen in earlier classical trajectory caculations[28] though the underlying reasons were not identified.

The resulting rotational distribution, in certain cases, may be strikingly similar to that of the rotational Boltzmann plot, and this has led authors to attempt to fit data in a Boltzmann simulation and to extract a rotational "temperature". The analysis presented here suggests that this is likely to be a misleading procedure since the distribution is more accurately described as frustrated exponential-like. This arises through the channel selective reduction in maximum value of $b_n$ that will allow the mechanism to operate in the presence of an energy constraint. This shifts the peak of the $\Delta j$ distribution away from zero to a value dependent on kinematic factors and the vibrational momentum gap.

In this work, three examples are shown to illustrate the predictability of the peak shifts for systems as diverse as $Li_2$−Ne, NO−NO, and HF−H*. In the first of these, the vibrational momentum gap is relatively small and the effect of energy constraints in this case is mainly to suppress the $\Delta j = 0$ process. The similarity to an exponential-like distribution is more clearly evident in these data than in any other considered here. The vibrational momentum gap in NO is much larger than in $Li_2$, and a greater peak shift is anticipated. The collision partner in this case (NO in its vibrational ground state) brings its own characteristic vibrational momentum to the interaction, which has the effect of enhancing strongly the $\Delta j = -1$ rate constant due to a momentum "resonance". Note that it is not necessary to invoke a long range multipolar interaction in order to explain this behavior and the uniformity of collisional mechanism may be sustained. HF has a very large momentum gap, and as a consequence, the low $\Delta j$ region of the rotational distribution is strongly suppressed. This leads to a distribution shape that is deceptively similar to a rotational Boltzmann, but it will be clear from the foregoing that this similarity is misleading.

The underlying physics of the collisional process in each case is very clearly revealed in velocity−AM plots which are graphical representations both of the basic mechanism of LM → AM conversion and of the manner in which this is influenced by the boundary conditions set by energy conservation (eqs 1 and 2). These, in conjunction with our knowledge of the functional form of $P(\Delta j)$ (eq 3), allow simple, accurate, rule-of-thumb estimates of the shape and the peak of the rotational distributions in VRT. A key element in this representation is the treatment of molecular vibration as (reciprocating) momentum and in atom−diatom VRT; this momentum must be overcome before rotational AM may be induced. When the collision partner is also a diatomic molecule, this brings its characteristic vibrational momentum, which projects the distribution of relative collision velocities to higher velocities. In certain cases (e.g., for the NO−NO encounters considered here) this is sufficient to open the vibrational channel. In other instances, this may not be the case despite achieving "near energy degeneracy", a prerequisite for efficient VRT in the long-range model.

This approach provides a consistent physical picture of VRT collisions and establishes the processes considered here to be

identical in mechanism to pure RT[4,5,14] and to QRT.[12,13] Only the boundary conditions of energy conservation vary from process to process though these are readily incorporated into a quantitative determination of VRT distributions.[7] We have shown that the same basic mechanism accounts well for reactive collisions[19] with relatively straightforward modifications to account for change of center-of-mass and to include the contribution from reaction enthalpy. No recourse is made in the model to details of the intermolecular potential except insofar that atomic and molecular *sizes* are related to the onset of the repulsive wall and that bond lengths represent a measure of repulsive anisotropy. The velocity−AM plots shown above and used in this analysis require nothing more sophisticated than atomic masses, radii, bond lengths, and spectroscopic data. Multiellipsoid Monte Carlo trajectory calculations based on these physical priciples[7,14,19,21] accurately reproduce experimental cross sections emphasizing once again the central role played by the molecule's physical shape in this model.

Two additional points may be made relating to the experimental determination of rate constants or cross sections for vibrational transfer using laser-spectroscopic methods. First, it is important, as Stewart and co-workers have shown,[9] that the probabilities to all rotational states of the final vibrational state are summed. Failure to accomplish this may not necessarily lead to large inaccuracies, depending on such factors as the wavelength spread of the rotational lines and on the intensity distribution among them. Second, it is clear that additional energetic constraints arise when $j_i \neq 0$ and that this effect is magnified when the energy gaps for unit AM change become very large. This effect is further amplified when reduced mass increases and will strongly affect comparative determinations. These two effects suggest strongly that VT studies should focus on (i) careful selection of $j_i \simeq 0$ and (ii) summing the contributions of all rotational states in the final vibrational level in order that accurate vibrational transfer rate coefficients be obtained. This is particularly important when variation over a range of collision partners is the subject of the investigation.

## References and Notes


(1) Levine, R. D.; Bernstein, R. B. *Molecular Reaction Dynamics and Chemical Reactivity*; Oxford University Press: New York, 1987.

(2) Klatt, M.; Smith, I. W. M.; Symonds, A. C.; Tuckett, R. P.; Ward, G. N. *J. Chem. Soc., Faraday Trans.* **1996**, *92*, 193.

(3) Murrell, J. N.; Bosanac, S. D. *Introduction to the Theory of Atomic and Molecular Collisions*; John Wiley: Chichester, U.K., 1989; p 50.

(4) McCaffery, A. J.; AlWahabi, Z. T.; Osborne, M. A.; Williams, C. J. *J. Chem. Phys.* **1993**, *98*, 4586.

(5) Osborne, M. A.; McCaffery, A. J. *J. Chem. Phys.* **1994**, *101*, 5604.

(6) Osborne, M. A.; Marks, A. J.; McCaffery, A. J. *J. Phys. Chem.* **1996**, *100*, 3888.

(7) Clare, S.; Marks, A. J.; McCaffery, A. J. *J. Chem. Phys.* **1999**, *111*, 9287.

(8) Islam, M.; Smith, I. W. M. *J. Chem. Phys.* **1999**, *111*, 9296.

(9) Gao, Y.; Gorgone, P. S.; Davies, S.; McCall, E. K.; Stewart, B. *J. Chem. Phys.* **1996**, *104*, 1415. Gao, Y.; Stewart, B. *J. Chem. Phys.* **1995**, *103*, 860.

(10) Lindner, J.; Lundberg, J. K.; Lovejoy, C. M.; Leone, S. R. *J. Chem. Phys.* **1997**, *106*, 2265.

(11) O'Neill, J. A.; Wang, C. X.; Cai, J. Y.; Flynn, G. W.; Weston, R. E. *J. Chem. Phys.* **1988**, *88*, 6240. Khan, F. A.; Kreutz, T. G.; O'Neill, J. A.; Wang, C. X.; Flynn, G. W.; Weston, R. E. *J. Chem. Phys.* **1990**, *93*, 445. Khan, F. A.; Kreutz, T. G.; Flynn, G. W.; Weston, R. E. *J. Chem. Phys.* **1990**, *92*, 4876.

(12) McCaffery, A. J. *J. Chem. Phys.* **1999**, *111*, 7697.

(13) Clare, S.; McCaffery, A. J. *J. Phys. B.* **2000**, *33*, 1121.

(14) Clare, S.; Marks, A. J.; McCaffery, A. J. *J. Phys. Chem.* **2000**, *104*, 7181.

(15) Besley, N. A.; McCaffery, A. J.; Osborne, M. A.; Rawi, Z. *J. Phys. B* **1998**, *31*, 4267.

(16) Mack, J. A.; Mikulecky, K.; Wodtke, A. M. *J. Chem. Phys.* **1996**, *105*, 4105.

(17) McCaffery, A. J.; Wilson, R. J. *J. Phys. B* **1997**, *30*, 5773. McCaffery, A. J.; Wilson, R. J. *Phys. Rev. Lett.* **1996**, *77*, 48.

(18) McCaffery, A. J.; Truhins, K.; Whiteley, T. W. J. *J. Phys. B* **1998**, *31*, 2023.

(19) Marsh, R.; McCaffery, A. J.; Truhins, K.; Whiteley, T. *J. Chem. Phys.* **2000**, *112*, 5281.

(20) Kreutz, T. G.; Flynn, G. W. *J. Chem. Phys.* **1990**, *93*, 452.

(21) Marks, A. J. *J. Chem. Soc., Faraday Trans.* **1994**, *94*, 2857.

(22) Hoffbauer, M. A.; Burdenski, S.; Giese, C. F.; Gentry, W. R. *J. Chem. Phys.* **1983**, *78*, 3832.

(23) Polanyi, J. C.; Woodall, K *J. Chem. Phys.* **1972**, *56*, 1563.

(24) Brunner, T. A.; Pritchard, D. E. *Adv. Chem. Phys.* **1982**, *50*, 589.

(25) Parmenter, C. S.; Clegg, S. M.; Krajnovitch, D. J.; Lu, S. P. *Proc. Natl. Acad. Sci.* **1997**, *94*, 8387.

(26) Stewart, B.; Magill, P. D.; Scott, T. P.; Derouard, J.; Pritchard, D. E. *Phys. Rev. Lett.* **1988**, *60*, 282.

(27) Sharma, R. D.; Brau, C. *Phys. Rev. Lett.* **1967**, *19*, 1273. Sharma, R. D. *J. Chem. Phys.* **1968**, *49*, 5195; *Phys. Rev.* **1969**, *177*, 102.

(28) See for example Thompson, D. L. *J. Phys. Chem.* **1982**, *86*, 2538. Serri, J. A.; Bilotta, R. M.; Pritchard, D. E. *J. Chem. Phys.* **1982**, *77*, 2940.